Duration of the Arctic Sea Ice Melt Season: Regional and Interannual Variability, 1979–2001

G. I. BELCHANSKY

Space Monitoring and Ecoinformation Systems Sector, Institute of Ecology, Russian Academy of Sciences, Moscow, Russia

D. C. DOUGLAS

U.S. Geological Survey Alaska Science Center, Juneau Field Station, Juneau, Alaska

N. G. PLATONOV

Space Monitoring and Ecoinformation Systems Sector, Institute of Ecology, Russian Academy of Sciences, Moscow, Russia

(Manuscript received 19 February 2003, in final form 11 June 2003)

ABSTRACT

Melt onset dates, freeze onset dates, and melt season duration were estimated over Arctic sea ice, 1979–2001, using passive microwave satellite imagery and surface air temperature data. Sea ice melt duration for the entire Northern Hemisphere varied from a 104-day minimum in 1983 and 1996 to a 124-day maximum in 1989. Ranges in melt duration were highest in peripheral seas, numbering 32, 42, 44, and 51 days in the Laptev, Barents-Kara, East Siberian, and Chukchi Seas, respectively. In the Arctic Ocean, average melt duration varied from a 75-day minimum in 1987 to a 103-day maximum in 1989. On average, melt onset in annual ice began 10.6 days earlier than perennial ice, and freeze onset in perennial ice commenced 18.4 days earlier than annual ice. Average annual melt dates, freeze dates, and melt durations in annual ice were significantly correlated with seasonal strength of the Arctic Oscillation (AO). Following high-index AO winters (January–March), spring melt tended to be earlier and autumn freeze later, leading to longer melt season durations. The largest increases in melt duration were observed in the eastern Siberian Arctic, coincident with cyclonic low pressure and ice motion anomalies associated with high-index AO phases. Following a positive AO shift in 1989, mean annual melt duration increased 2–3 weeks in the northern East Siberian and Chukchi Seas. Decreasing correlations between consecutive-year maps of melt onset in annual ice during 1979–2001 indicated increasing spatial variability and unpredictability in melt distributions from one year to the next. Despite recent declines in the winter AO index, recent melt distributions did not show evidence of reestablishing spatial patterns similar to those observed during the 1979–88 low-index AO period. Recent freeze distributions have become increasingly similar to those observed during 1979–88, suggesting a recurrent spatial pattern of freeze chronology under low-index AO conditions.

1. Introduction

Knowledge about sea ice distribution, ice type, melt dynamics, and their integrated influence on sea ice shortwave albedo, is critical for understanding mechanisms of global climate (Barry et al. 1993; Barry 1996). Sea ice melt dynamics are important factors of climate change because the time of melt onset, melt ponding, and freeze are associated with meaningful alterations in the shortwave albedo of the broad-scale environment (Perovich 1996). Decreasing albedo increases shortwave absorption and accelerates snow and sea ice melting through positive feedback (Curry et al. 1995). Associated changes in surface heat flux caused by changes in sea ice cover ultimately influence energy balances and feedbacks of the atmosphere–ocean–ice system (Mysak and Venegas 1998; Ikeda et al. 2001). Consequently, understanding seasonal sea ice melt and albedo dynamics, including regional and interannual variability, is important for improving climate simulation models (Parkinson 1992; Chapman and Walsh 1993; Maslanik et al. 1996; Barry 1996; Deser et al. 2000; Steele et al. 2001; Comiso 2001).

Distinctive radiative and surface characteristics of sea ice during summer facilitate studies of melt using optical and microwave satellite data (Parkinson 1992; Comiso and Kwok 1996; Pettersson et al. 1996; Yackel and Barber 2000). Several methods have been developed to estimate melt onset dates that utilize passive microwave brightness temperature (T_b) data (Serreze et al. 1993;

Corresponding author address: D. C. Douglas, U.S. Geological Survey Alaska Science Center, Juneau Field Station, 3100 National Park Road, Juneau, AK 99801.
E-mail: david_douglas@usgs.gov

Abdalati and Steffen 1997; Anderson 1997; Smith 1998a; Drobot and Anderson 2001a), but studies of freeze onset and melt duration are few and have been limited to perennial ice (Smith 1998a, 1998b).

The Arctic Oscillation (AO) index (Thompson and Wallace 1998) is a commonly used parameter for characterizing alternating high and low pressure anomalies over the Arctic. The AO is constructed by projecting the daily (0000 UTC) 1000-mb height anomalies poleward of 20°N onto the loading pattern of the AO. The loading pattern of the AO is defined as the leading mode of empirical orthogonal function analysis of monthly mean 1000-mb height during 1979–2000. Under high-index AO conditions, sea level pressures over the central Arctic Ocean are substantially lower and vorticity of the gradient wind fields are more cyclonic (Walsh et al. 1996).

Decadal oscillations in Arctic atmospheric circulation have been correlated with observational changes in sea ice motion (Zhang et al. 2000; Rigor et al. 2002), surface air temperature (Rigor et al. 2000), melt season onset (Drobot and Anderson 2001b), and summer ice cover (Maslanik et al. 1996; Yi et al. 1999; Deser et al. 2000). More frequent low pressure systems in the eastern Arctic during high-index AO periods have been associated with cyclonic sea ice motion anomalies, warmer surface air temperatures, earlier melt, and reduced summer ice cover.

Our investigation of melt duration contributes to a growing body of evidence linking atmospheric processes with changes in the Arctic sea ice environment. In this paper, we estimate melt onset dates, freeze onset dates, and duration of the melt season over Arctic sea ice, 1979–2001, using a new method of passive microwave data analysis that interrogates surface air temperature (SAT) data to control anomalies. We examine relationships between ice melt dynamics and seasonal strength of the AO, compare our results to those obtained using other published methods, and analyze sensitivities of algorithm output to changes in the algorithm thresholds and T_b calibration coefficients.

2. Methods

a. Data

Gridded (25-km pixel resolution) T_b and derivative sea ice concentration databases were obtained from the National Snow and Ice Data Center (NSIDC): *Nimbus-7* Scanning Multichannel Microwave Radiometer (SMMR) Radiance and Sea Ice Concentrations (Gloerson et al. 1990), Defense Meteorological Satellite Program (DMSP) Special Sensor Microwave Imager (SSM/I) Daily Gridded Brightness Temperatures (Maslanik and Stroeve 1990–2001), and SSM/I Average Daily Polar Gridded Sea Ice Concentrations (Comiso 1990–2001). We constructed a consistent 23-yr record of SMMR–SSM/I T_b data by standardizing among instruments based on periods of overlap, reducing the influences of coastal boundaries, eliminating bad data, and interpolating missing data (Cavalieri et al. 1999). Linear regression coefficients were applied to standardize intersatellite T_b measurements to the DMSP *F8* SSM/I instrument: *Nimbus-7* SMMR to *F8* SSM/I (Jezek et al. 1991); *F13* SSM/I to *F11* SSM/I (Stroeve et al. 1998); and *F11* SSM/I to *F8* SSM/I (Abdalati et al. 1995). Pixels with invalid data for one or more channels were omitted, missing data were filled by spatial or temporal linear interpolation (Cavalieri et al. 1999), and missing SSM/I data from 3 December 1987 to 13 January 1988 were filled with modeled values using the multiple ordinary least squares regression method described by Gloerson et al. (1999).

Twice daily (12 h) SAT maps, 1979–2000, in stereographic projection with 100-km pixel resolution, were obtained from the International Arctic Buoy Program/Polar Exchange at the Sea Surface (IABP/POLES; Rigor et al. 2000). The digital SAT maps complemented the SMMR–SSM/I T_b data by independent measurement of daily thermal conditions throughout the Arctic. We created daily (24 h) 25-km pixel resolution maps for coanalyses with the T_b grids by averaging and interpolating, respectively. Daily maps of smoothed air temperatures (14-day interval, 7 days before and 6 days after) were also constructed by averaging the 24-h maps prior to the 25-km interpolation.

Average monthly standardized values of the Arctic Oscillation (Thompson and Wallace 2000) were obtained from http://horizon.atmos.colostate.edu/ao/ to investigate correlations between annual sea ice melt dynamics and strength of the Northern Hemisphere annular mode. Comparisons between methods of estimating melt and freeze dates were made during time intervals when respective data were available.

b. Study area

The study area included all pelagic pixels (beyond two pixels from the coastline) in the Northern Hemisphere where ≥50% winter (January–March) ice cover (Comiso 1990–2001) persisted throughout the 23-yr time series (Fig. 1). Results were summarized regionally following delineations presented in Parkinson et al. (1999): Arctic Ocean, Barents-Kara Sea, Laptev Sea, East Siberian Sea, and Chukchi Sea. Within the Arctic Ocean, results were partitioned for two ice types: perennial ice and annual ice. An Arctic Ocean pixel dominated by multiyear ice (Comiso 1990–2001) during winter for a majority of years (1988–99) was classified as perennial ice, otherwise as annual ice.

c. Algorithms

We developed new algorithms for estimating melt and freeze dates from SMMR–SSM/I T_b data that were premised on Drobot and Anderson's (2001a) Advanced

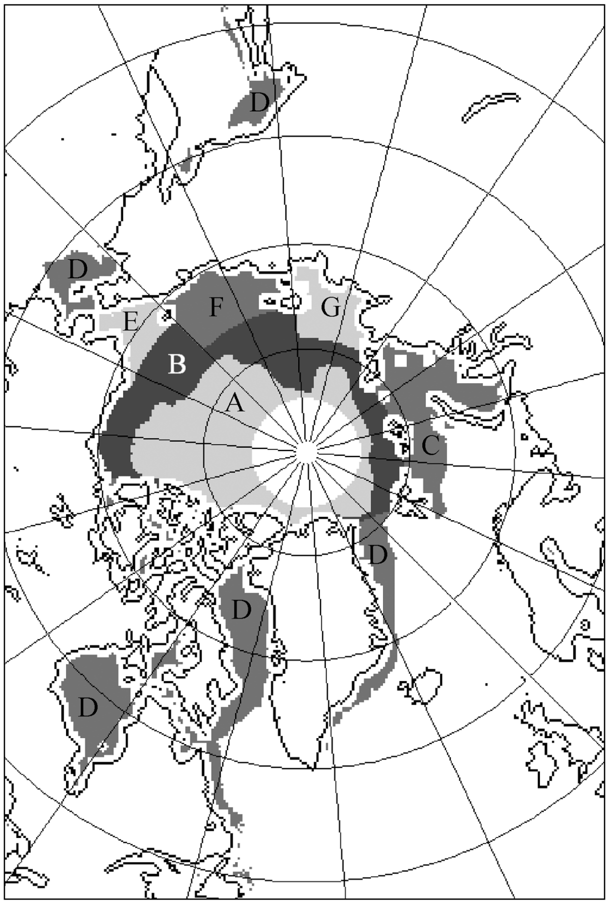

FIG. 1. Regional study areas: Northern Hemisphere (A, B, C, D, E, F, G), Arctic Ocean (A, B, E, F, G), Barents and Kara Seas (C), Chukchi Sea (E), East-Siberian Sea (F), Laptev Sea (G), Arctic Ocean perennial sea ice (A), and Arctic Ocean annual sea ice (B, E, F, G).

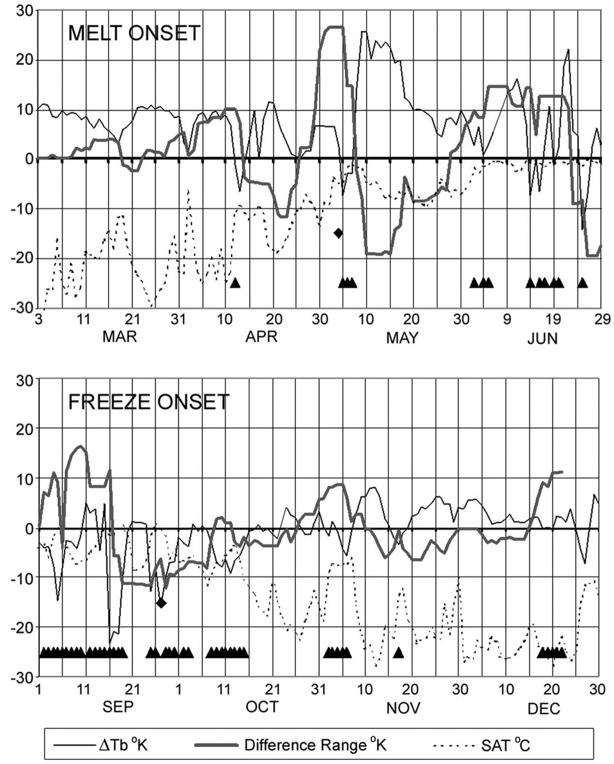

FIG. 2. Potential dates of melt and freeze onset (baseline triangles) vs the melt and freeze onset data selected by the PMSTA (elevated diamond) for an arbitrary location in the Barents Sea, 1989, plotted with corresponding evolutions of SSM/I ΔT_b (19H − 37H), difference range, and IABP/POLES SAT.

Horizontal Range Algorithm (AHRA). To circumvent spurious melt onset estimates, we enhanced the AHRA to interrogate the IABP/POLES SAT databases. We also elaborated the AHRA to analyze T_b and SAT measurements in reverse chronology for estimating freeze onset dates.

To estimate melt onset, the AHRA evaluates: [(max2 ΔT_b − min2 ΔT_b) − (max1 ΔT_b − min1 ΔT_b)], where ΔT_b is the daily difference between the horizontally polarized (H) 18.0-GHz (or 19.3-GHz for SSM/I) and 37.0-GHz H channels over the previous 10-day (max1, min1) and subsequent 9-day (max2, min2) periods (Drobot and Anderson 2001a). SMMR ΔT_b and SSM/I ΔT_b change from positive to near-zero or negative during the melt season because 18.0-GHz H and 19.3-GHz H T_b values are more responsive to melting processes than 37.0-GHz H T_b values (Onstott et al. 1987; Anderson 1997). The AHRA calculates ΔT_b as function of each day, and performs the following tests for each pixel that is dominated by sea ice: 1) if $\Delta T_b > 4$ K, then winter conditions; 2) if $\Delta T_b \leq -10$ K, then melt onset conditions; 3) if -10 K $< \Delta T_b \leq 4$ K and [(max2 ΔT_b − min2 ΔT_b) − (max1 ΔT_b − min1 ΔT_b)] $>$ 7.5 K, then melt onset conditions.

To circumvent spurious AHRA estimates, we constrained the algorithm to periods with compatible thermal regimes based on the IABP/POLES average daily SAT maps. For each pixel, the first date after 1 April that SAT exceeded -5°C was determined, and the AHRA was applied henceforth. The first subsequent date to pass melt condition criteria was recorded as the melt onset date for the respective year. To estimate annual freeze onset date, the AHRA was executed in reverse chronology using different thresholds. Beginning 31 December, and using a ≥ -2°C surface air temperature constraint, the AHRA was applied with the following conditional tests: 1) if $\Delta T_b > 5$ K, then winter conditions; 2) if $\Delta T_b \leq -3$ K, then freeze onset date; 3) if -3 K $< \Delta T_b \leq 5$ K and [(max2 ΔT_b − min2 ΔT_b) − (max1 ΔT_b − min1 ΔT_b)] $>$ 7.5 K, then freeze onset date. We subsequently refer to our integrated algorithm as the Passive Microwave Surface Temperature Algorithm (PMSTA).

Evolutions of SAT, ΔT_b, and the T_b difference range [(max2 ΔT_b − min2 ΔT_b) − (max1 ΔT_b − min1 ΔT_b)] during the 1989 melt and freeze seasons are illustrated in Fig. 2 for an arbitrary location in the Barents Sea (79.70°N, 37.87°E). In this example, 12 April was iden-

TABLE 1. Mean annual Julian dates of melt onset, freeze onset, and duration of the melt season, 1979–2001, for the Northern Hemisphere, Arctic Ocean, and peripheral seas, and perennial and annual ice types within the Arctic Ocean.

Region	Melt onset date		Freeze onset date		Melt duration	
	Mean	Std dev (days)	Mean	Std dev (days)	Mean	Std dev (days)
Northern Hemisphere	152	3.4	263	3.4	112	5.7
Barents–Kara Seas	145	7.6	272	4.8	127	9.8
Chukchi Sea	146	10.5	270	7.3	124	11.2
Laptev Sea	156	5.5	259	5.8	103	8.0
East Siberian Sea	159	6.2	259	6.8	100	10.9
Arctic Ocean	163	4.2	249	4.6	86	7.0
Perennial ice	170	4.3	236	5.3	66	7.9
Annual ice	159	5.0	256	5.8	97	8.3

tified as the first (earliest) potential melt onset date based on T_b signatures, but the PMSTA rejected 12 April because spring SAT had not reached $-5°C$. The next date with a valid T_b melt signature (4 May) complied with the SAT threshold and was selected by the PMSTA as the melt onset date. Although subsequent dates passed all criteria, the PMSTA selected the earliest. Moving in reverse chronology during autumn (Fig. 2), several potential freeze dates were identified based on their T_b signatures, but the $-2°C$ PMSTA SAT threshold rejected all candidates until 26 September.

The $-5°C$ SAT melt onset threshold imposed by the PMSTA was chosen by comparing pixels with anomalously early AHRA estimates to corresponding temporal evolution of IABP/POLES daily SAT. The SAT threshold was determined by selecting a temperature high enough to circumvent a majority of spurious AHRA estimates, but low enough to allow robust detection of melt onset by the daily T_b signatures. In practice, the $-5°C$ threshold prevented the melt onset date from occurring prior to the first spring occurrence of SAT $> -5°C$.

The T_b and SAT thresholds for estimating freeze onset were chosen by analyzing coincident *Okean-1* radar, IABP/POLES SAT, and SSM/I T_b data, 1995–1998. Characteristic changes in *Okean-1* backscatter associated with freeze conditions (Belchansky and Douglas 2002) were used to partition and quantify SAT and T_b behaviors during freeze transitions. The PMSTA T_b and SAT thresholds were chosen to maximize concurrence

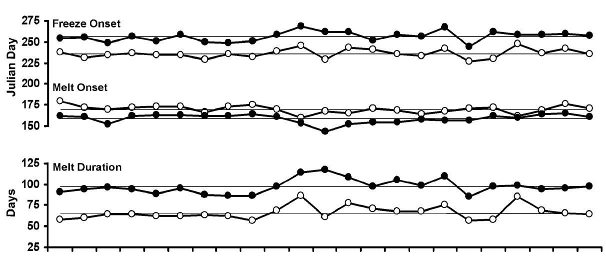

FIG. 3. Annual mean melt onset date, freeze onset date, and duration of the melt season in annual ice (solid) and perennial ice (open), Arctic Ocean, 1979–2001. Horizontal lines reference 23-yr averages.

with the *Okean-1* backscatter freeze signatures, and with *ERS-1* synthetic aperture radar (SAR) estimated freeze-up dates presented in Smith (1998a). The $-2°C$ threshold prevented the freeze onset date from occurring after the last autumn occurrence of SAT $> -2°C$.

Melt and freeze onset dates were also estimated solely from the IABP/POLES SAT data, following the approach presented in Rigor et al. (2000). The melt onset date was defined as the first date after 1 April to exceed $-1.0°C$ in the 14-day smoothed average daily surface air temperature maps. In reverse chronology, the first day preceding 31 December to exceed $-1.0°C$ was identified, and the subsequent day was defined as the freeze onset date.

3. Results and discussion

a. Chronology and distribution

Mean dates of melt onset, freeze onset, and duration of the melt season varied among years and between regions (Table 1). On average, melt began in the peripheral seas during late May and early June, then advanced rapidly over the Arctic Ocean reaching the pole near the end of the third week of June. Freeze onset at the northernmost latitudes began, on average, during the fourth week of August, reaching the East Siberian and Laptev Seas in mid-September, and the Chukchi, Barents, and Kara Seas in late September.

Annual melt duration in the Northern Hemisphere 1979–2001 varied from a 104-day minimum in 1983 and 1996, to a 124-day maximum in 1989. Ranges in melt duration were highest in peripheral seas, numbering 32, 42, 44, and 51 days in the Laptev, Barents–Kara, East Siberian, and Chukchi Seas, respectively. In the Arctic Ocean, melt duration varied from a 75-day minimum season in 1987 to a 103-day maximum in 1989.

On average, annual ice began to melt 10.6 days earlier (std dev = 4.6) and freeze 18.4 days later (std dev = 4.6) than perennial ice (Fig. 3). Melt duration in annual ice averaged 30.6-days longer (std dev = 6.9) than perennial ice, and was relatively constant over the 23-yr record. Notable exceptions were 1990 when melt du-

Table 2. Correlations (r) between the AO index (winter, January–March and late summer, July–September) and mean sea ice melt onset date, freeze onset date, and melt season duration, 1979–2001, for the Northern Hemisphere, Arctic Ocean, and peripheral seas, and perennial and annual ice types within the Arctic Ocean. Significant ($S \geq 95\%$, $|r| > 0.42$) product–moment correlation coefficients are shown in bold type.

Region	Jan–Mar AO			Jul–Sep AO	
	Melt	Freeze	Duration	Freeze	Duration
Northern Hemisphere	**−0.55**	**0.45**	**0.60**	0.38	0.26
Barents–Kara Seas	**−0.54**	0.14	**0.49**	0.14	0.12
Chukchi Sea	−0.31	−0.06	0.24	0.14	0.17
Laptev Sea	−0.21	0.31	0.37	**0.65**	0.33
East Siberian Sea	**−0.49**	**0.45**	**0.64**	**0.44**	0.19
Arctic Ocean	**−0.57**	**0.52**	**0.66**	**0.42**	0.36
Perennial ice	−0.37	0.25	0.37	0.29	0.37
Annual ice	**−0.60**	**0.55**	**0.74**	0.41	0.29

ration in annual ice was 49 days longer than perennial ice, and 1998 when only 13 days longer.

b. Associations with the Arctic Oscillation

Average annual melt and freeze onset dates, and melt season duration, were significantly correlated with the Arctic Oscillation index (Table 2). Following high-index AO winters (January–March), spring melt tended to be earlier and autumn freeze later, leading to longer melt seasons. Correlations with the AO were strongest for annual ice in the Arctic Ocean, especially in the East Siberian Sea. Freeze onset dates were also correlated with the AO during late summer (July–September) in the East Siberian and Laptev Seas, where high-index AO conditions were associated with delayed freeze. Correlations between the AO and melt dynamics in perennial ice were not statistically significant (Table 2).

Melt duration in the Arctic Ocean dramatically increased concurrent with a pronounced positive phase shift in the winter AO during the late 1980s (Fig. 4). Subsequently, melt duration generally decreased along with an overall weakening trend in the winter AO. Melt duration in annual ice was more closely associated with the winter AO index, compared to perennial ice (Fig. 4, Table 2). In perennial ice, melt duration more or less adhered to the AO's decadal frequency, but prominent annual disassociations (e.g., 1998) contributed to insignificant correlations.

Sea ice melt and freeze distributions, before (1979–88) and after (1989–2001) the AO positive phase shift, are spatially illustrated in (Fig. 5). Northward expansions of earlier melt and later freeze during the high-index AO period were most apparent in the northern East Siberian and Chukchi Seas. In general, sea ice began melting earlier and freezing later throughout most of the Arctic during the high-index AO period. However, in the Eurasian Arctic Ocean (20°–140°E) poleward of 80°N, somewhat later sea ice melt during the high-index AO period was offset by much later freeze, resulting in slightly longer average melt duration.

Cyclonic wind fields over the Siberian sector of the Arctic Ocean were more prevalent during the high-index AO period, and coincided with the area of greatest increase in melt season duration (Fig. 6). In the northern East Siberian and Chukchi Seas, mean annual melt duration was 2–3-weeks longer after the AO shifted to a more positive phase, compared to prior years. Within this region of pronounced and contiguous change (72.5°–80°N, 160°W–160°E), melt onset averaged 9.6 days earlier, and freeze onset averaged 10.6 days later, during the high-index AO period (Table 3). Longer, less pronounced melt seasons occurred in the Barents Sea, areas north of the New Siberian Islands, and northwest of the Canadian Archipelago.

Low pressure systems in the eastern Arctic establish wind-forcing patterns that contribute to earlier melt by advection of warmer southerly air into the East Siberian and northern Chukchi Seas (Serreze et al. 1995; Maslanik et al. 1996). High-index AO winters have been associated with pronounced SAT warming trends during spring (Rigor et al. 2000), earlier melt onset dates in the East Siberian Sea (Drobot and Anderson 2001a, 2001b), and longer melt seasons in the eastern Arctic (Rigor et al. 2000). Lower concentrations of summer ice cover in the Siberian arctic also occurred during periods with higher frequencies of low pressure systems (Maslanik et al. 1996; Deser et al. 2000).

During high-index AO winters, a greater prevalence of cyclonic wind fields force cyclonic sea ice motion anomalies that reduce ice transport into the eastern Arctic and increase divergence within (Zhang et al. 2000; Rigor et al. 2002), promoting formation of thin ice and open leads (Rigor et al. 2002). Warm SAT anomalies observed in the eastern Arctic during high-index AO winters (Rigor et al. 2000) were attributed, in part, to both increased latent heat released during formation of new ice and increased sensible heat flux through thinner ice (Rigor et al. 2002). A greater abundance of open water, leads, and thin ice enhances heat flux from water, decreases surface albedo and amplifies the summer melt through positive feedbacks (Curry et al. 1995; Rigor et al. 2000; Zhang et al. 2000). Hence, both dynamic and thermodynamic processes associated with winter AO conditions can imprint signatures that persist later into the year through their influences on spring melt and

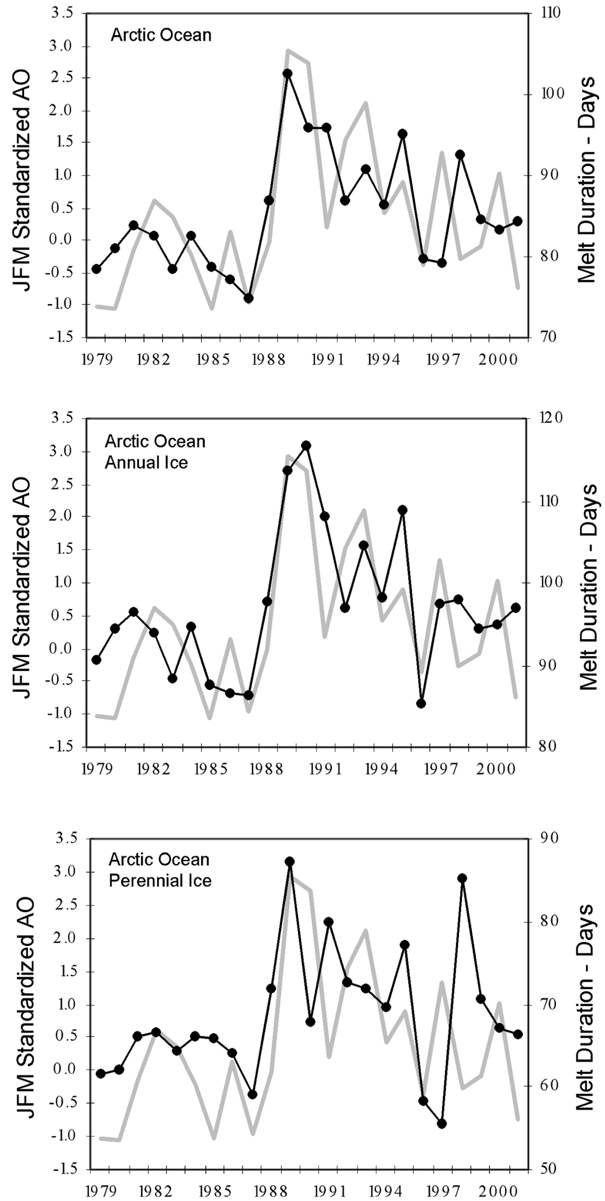

FIG. 4. Annual mean winter (Jan–Mar) AO index, 1979–2001 (gray), and (top) the annual mean melt season duration of Arctic Ocean sea ice, (middle) annual sea ice within the Arctic Ocean, and (bottom) perennial sea ice within the Arctic Ocean.

summer feedbacks (Rigor et al. 2000, 2002). We consider these processes and feedbacks commensurate with the northward expansions of earlier melt dates and later freeze dates observed in the East Siberian and Chukchi Seas following the 1989 positive AO shift (Fig. 5).

Melt durations in both perennial and annual ice were less variable during the 1979–88 low-index AO period (Fig. 4), when dominant anticyclonic conditions (Fig. 6) would have maintained a cooler, more uniform climate throughout the Arctic. After high pressure stability gave way to more prevalent cyclonic activity in 1989, melt duration variability increased in both ice types (Fig. 4), but statistical correlations with the winter AO index were observed for annual ice only (Table 2).

Although melt duration in perennial ice generally followed the AO's decadal cycle from 1979 to 2001, a pronounced disparity in 1998 (Fig. 4) precluded correlation. The unusually long 1998 melt season in perennial ice was not accompanied by atypically high AO indices, before or during the melt season. In spring 1998, a powerful storm system in the north Pacific influenced melt conditions in the high-latitude region of perennial ice, but the AO's annular integration deemphasized its specific importance. A strong and extensive low pressure anomaly centered over the north Bering Sea during March and April expedited advection of warm southerly air into the high Canadian Arctic where surface air temperatures ranged 4°–8°C above average [National Centers for Environmental Protection–National Center for Atmospheric Research (NCEP–NCAR) 40-Year reanalysis]. In 1998, early melt onset in perennial ice was roughly synchronous with annual ice (Fig. 3), leading to a hemispherical melt pattern also described by Drobot and Anderson (2001a). Warm surface air temperature anomalies in the western Arctic persisted through August and September 1998, delaying freeze and further extending the melt season.

Shorter melt seasons during 1989–2001 were apparent only in limited areas in the central and far northwestern Beaufort Sea (Fig. 6). Despite reports of slight cooling trends in the western Arctic (Thompson and Wallace 1998; Rigor et al. 2000), we found mean melt onset in perennial ice during 1989–2001 to be significantly earlier, and melt duration significantly longer, compared to 1979–88 (Table 3). Parkinson (1992) and Rigor et al. (2000) reported a lengthening of the sea ice season in the western Arctic, however, Parkinson quantified ice concentration data (not melt) over a relatively short time series (1979–1986), and Rigor's trend was very weak and statistically insignificant. Our melt duration results were more consistent with Smith (1998b), who estimated that melt duration in perennial Arctic sea ice was linearly increasing 0.53 day yr^{-1} (Table 4), but with opposing contributions of earlier melt versus later freeze.

Correlations between consecutive-year melt onset and melt duration maps of annual ice decreased linearly during 1979–2001, suggesting an increasing trend of spatial unpredictability in melt chronology and duration from one year to the next (Figs. 7a,b). Recent melt distributions did not, however, show evidence of reestablishing similarity to the 1979–88 low-index AO period (Fig. 7d), indicating local-scale melt patterns were less dependent on winter AO conditions compared to the significant correlations observed at broader scales (Table 2). Freeze distributions in annual ice did not exhibit a linear trend among year-to-year correlations (Fig. 7c), but the time series was inversely correlated with the winter AO ($r = -0.44$, $S = 96\%$). Recent freeze distributions have become increasingly similar to those ob-

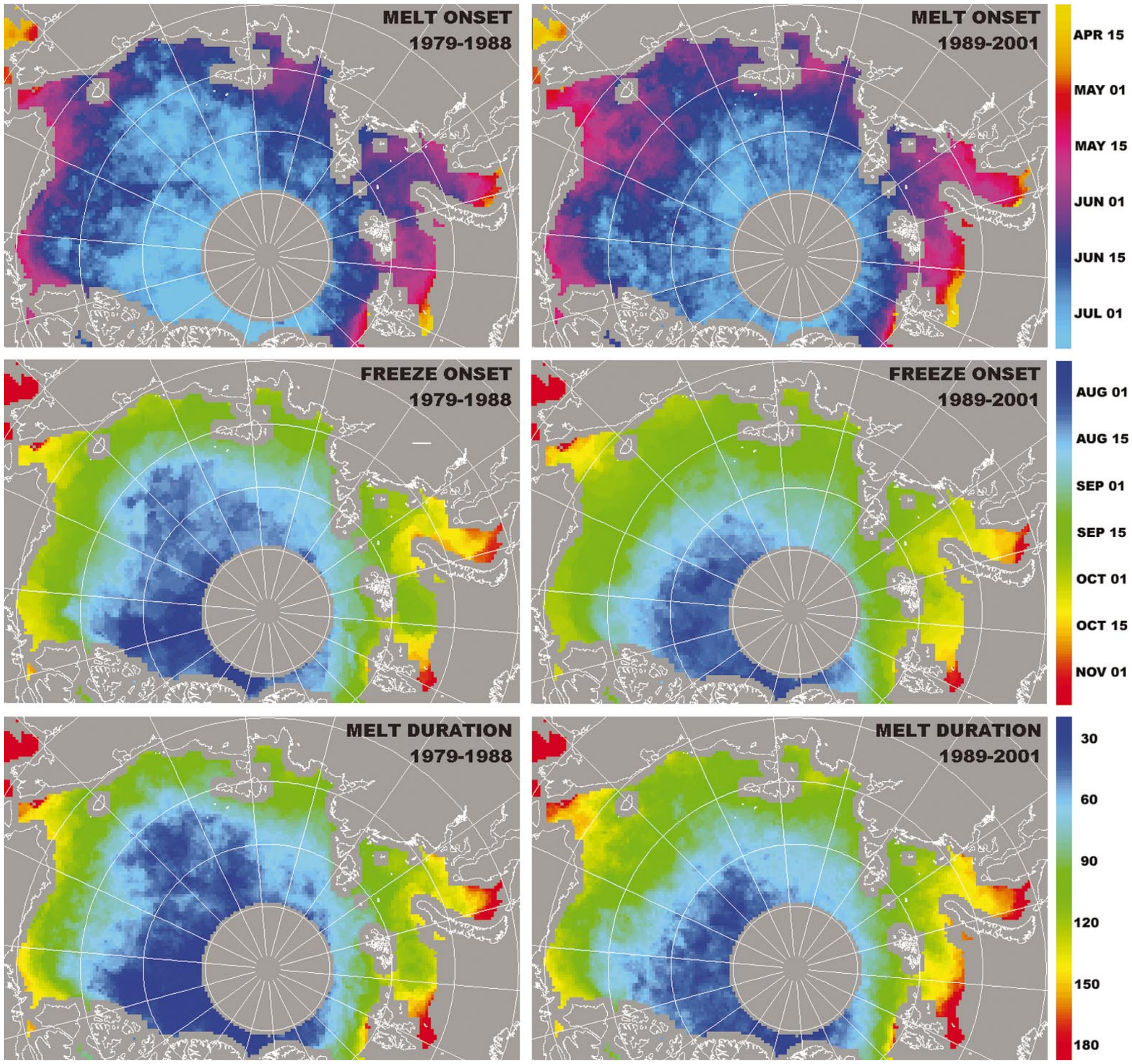

FIG. 5. Maps of average sea ice melt onset date, freeze onset date, and melt season duration in the Arctic Ocean and surrounding seas during the low-index AO period (1979–88) and high index AO period (1989–2001).

served during 1979–88 (Fig. 7d), indicating a recurrent spatial pattern of freeze chronology under low-index AO conditions. Because shortwave synoptic activity increases after the Arctic winter (Serreze et al. 1995), local-scale melt conditions would tend to experience higher interannual variability, compared to autumn when decreasing synoptic activity (especially prior to low-index AO winters) would tend to favor more stable and consistent local-scale freeze conditions.

c. Algorithm comparisons

Melt and freeze onset dates estimated by the PMSTA differed significantly from those obtained using only IABP/POLES SAT data, and from those disseminated in the NSIDC (AHRA method) melt onset database (Drobot and Anderson 2001c) (Table 5). The SAT data typically estimated later melt dates (except perennial sea ice), earlier freeze dates, and shorter melt durations compared to the PMSTA. Disparities between the PMSTA and SAT methods were largest in the peripheral seas, especially the Barents–Kara Sea.

Because sea ice melt and freeze are transitional processes (El Naggar et al. 1998), different detection methods are likely sensitive to different stages of transitional progression. Freeze onset dates defined by a <-1°C threshold in the smoothed IABP/POLES SAT data estimated early freeze conditions when air temperatures initially dropped. In contrast, the PMSTA evaluated T_b signatures that were sensitive to the disappearance of

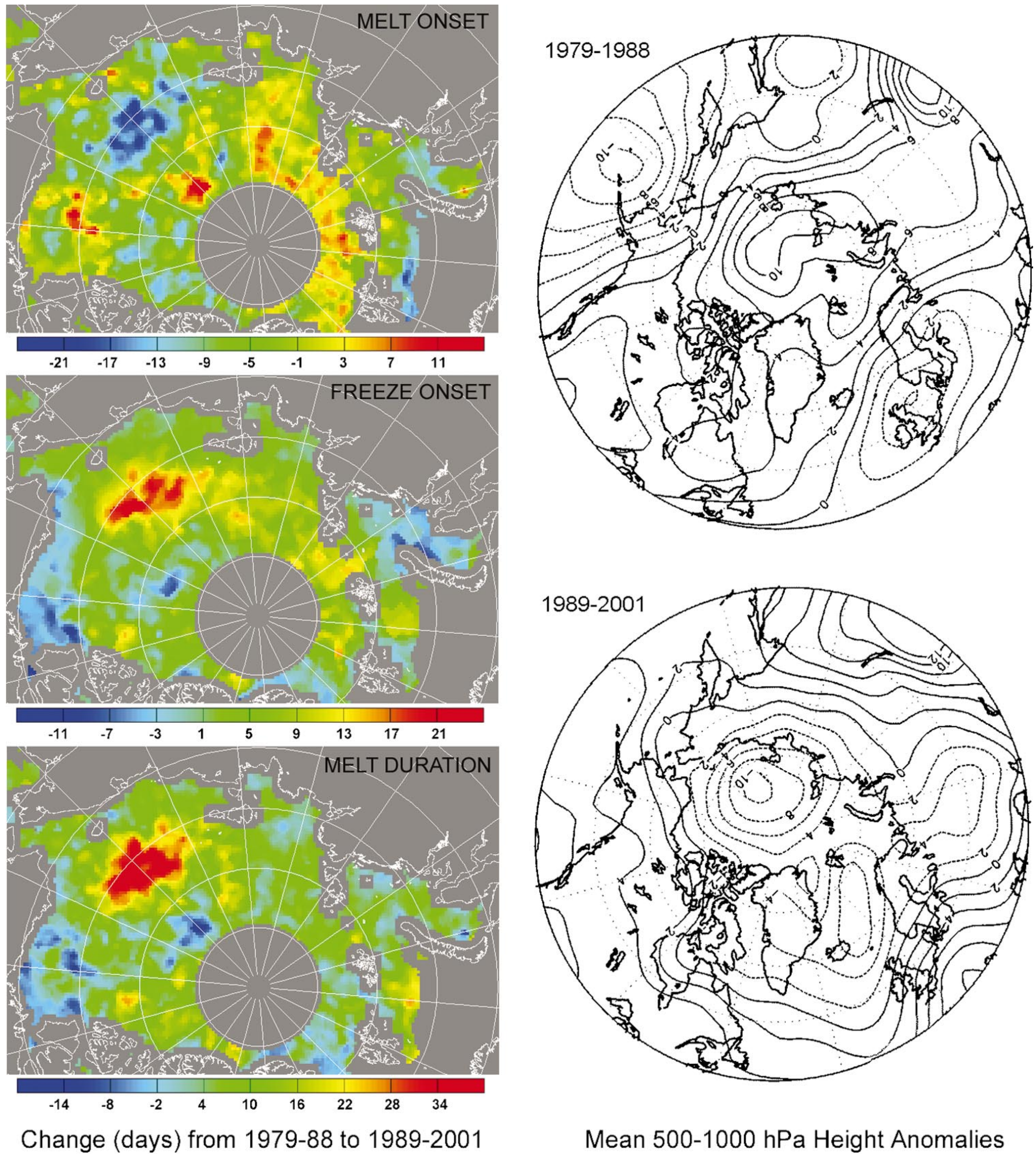

FIG. 6. Change in the mean (top left) melt onset, (middle left) freeze onset, and (bottom left) melt season duration (days), from 1979–88 to 1989–2001. Averaged 500–1000-hPa geopotential height anomalies: (top right) 1979–88 (bottom right) 1989–2001. Anomaly figures provided by the NOAA–CIRES Climate Diagnostics Center, Boulder, CO (available online at http://www.cdc.noaa.gov/).

liquid water (Anderson 1997), resulting in significantly later freeze estimates (Table 5). In the spring, the PMSTA detected earlier melt dates in the Chukchi, Laptev, and Barents–Kara Seas, likely caused by liquid water appearing in the snowpack well before surface air temperatures exceeded 0°C (Crane and Anderson 1994; Barber et al. 1995). However, an opposite melt relationship was observed in perennial ice (Table 5), indicating a latitudinal interaction between SAT and the initial appearance of liquid water (Fig. 8). On average, solar intensity at more northern latitudes is less capable of adding sufficient sensible heat to the snowpack to

TABLE 3. Mean change (Δ) in melt onset date, freeze date, and melt duration between years prior to the 1989 AO phase shift (1979–88), and years following the phase shift (1989–2001). Significant ($S \geq 95\%$) mean changes (t test) are shown in bold type.

Region	Melt onset date mean Δ	Freeze onset date mean Δ	Melt duration mean Δ
Northern Hemisphere	**−3.3**	**4.0**	**7.3**
Barents–Kara Seas	−5.1	2.3	7.4
Chukchi Sea	−5.1	0.3	7.4
Laptev Sea	−1.1	3.3	4.5
East Siberian Sea	**−8.8**	**5.9**	**14.7**
Arctic Ocean	**−3.8**	**5.0**	**8.6**
Perennial ice	**−4.2**	3.2	**7.4**
Annual ice	**−4.2**	**5.6**	**9.4**
72.5°–85°N, 160°W–160°E	**−9.6**	**10.6**	**20.2**

form liquid water under subzero air temperature conditions, thus requiring air temperatures to remain around 0°C before melt can commence (Drobot and Anderson 2001a). Although SAT and sea ice melt dynamics have strong latitudinal dependency, the coldest regions with the shortest melt seasons and most persistent ice cover are shifted from the pole toward the Canadian Archipelago and Greenland (Parkinson 1992; Smith 1998a; Rigor et al. 2000). This asymmetry contributed substantial variability to the latitudinal averages shown in Fig. 8.

The NSIDC melt onset database contained significantly earlier estimates throughout most of the Arctic compared to the PMSTA, and disparities were also greatest in the peripheral seas (Table 5). Although Drobot and Anderson (2001c) extracted the first melt date within a 9-point median filter to remove AHRA outliers when creating the NSIDC database, anomalous melt dates appeared to persist. Differences were pronounced in the Chukchi, Laptev, and Barents–Kara Seas, indicating that the AHRA's propensity to prematurely estimate melt onset was more prevalent in southern regions where solar radiation would be more likely to manifest singular ''melt events'' in the snowpack that misrepresented onset of the contiguous melt season. Confounding T_b signatures due to the appearance of open water by ice divergence (Smith 1998a) would also be more common in southern regions of marginal sea ice.

Both Smith (1998a) and Drobot and Anderson (2001a) evaluated their 1992 results at a set of 22 case sites (Winebrenner et al. 1994) in the northern Beaufort Sea in areas dominated by perennial ice. Average latitude among the 22 sites was 77.3°N (range 73.6°–81.6°N, std dev = 2.6°). When the 1992 PMSTA and IABP/POLES results were compared to the same case sites, differences among the methods (Table 6) were commensurate with the differences observed in perennial ice over longer periods and broader scales (Table 5). The PMSTA melt dates averaged 2.8 days later than Smith's (1998a), freeze onset differences were insignificant, and there were no latitudinal dependencies among the differences (Table 6).

All IABP/POLES melt onset comparisons revealed significant dependency with site latitude (Table 6). In general, the IABP/POLES melt date estimates were several days later at southern latitudes and several days earlier at northern latitudes, analogus to the interaction illustrated in Fig. 8. Freeze onset comparisons between IABP/POLES and Smith (1998a) also showed a latitudinal interaction, with the IABP/POLES method estimating later freeze in the south and earlier freeze in the north.

Accuracy of Smith's method was reported to be ±2 days and ±3 days for SSM/I-derived melt onset and freeze onset dates, respectively. Smith's method was found robust to instrument calibration, but reliable only in regions dominated by perennial ice. Although Smith's algorithm and data differed, mean estimates of melt and freeze dates were in general agreement with PMSTA method. The latitudinal interaction observed among comparisons with IABP/POLES method suggests the algorithm's uniform −1°C threshold may be oversimplified for defining melt and freeze throughout the entire Arctic. For northern regions of perennial ice, employing a warmer SAT spring threshold to accommodate more

TABLE 4. Mean melt and freeze dates (Julian day), mean melt duration (days), and respective linear trends, in perennial ice 1979–96, derived using the PMSTA and by Smith (1998b).

Perennial sea ice	PMSTA			Smith (1998b)		
	Mean (std dev)	Trend	S (%)	Mean	Trend	S (%)
Melt onset date	169(4.0)	−0.40 ± 0.16	97	164.49	−0.07	72.1
Freeze onset date	238(4.8)	+0.14 ± 0.23	46	239.61	+0.37	96.7
Melt duration	68(7.2)	+0.55 ± 0.32	90	75.05	+0.45	98.8
Number of melt days	—	—	—	65.47	+0.53	99.9

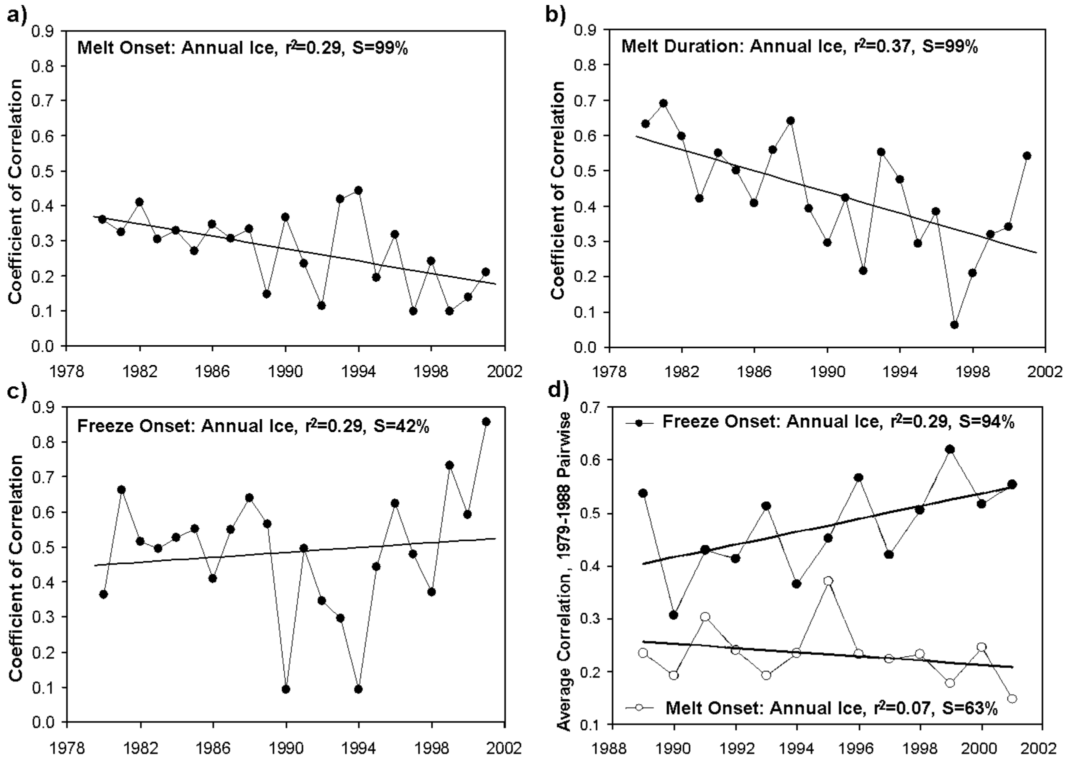

FIG. 7. Correlations between current and previous-year maps of annual sea ice in the Arctic Ocean, 1979–2001: (a) melt onset, (b) melt duration, (c) freeze onset, (d) average of all pairwise correlations (n = 10) obtained by correlating a melt (or freeze) onset map of annual ice in 1 yr during the high-index AO period (1989–2001) with respective maps in each and every year during the low-index AO period (1979–88).

time for the addition of sensible heat (Drobot and Anderson 2001a), and a colder SAT autumn threshold to allow release of latent heat, would better align the melt and freeze onset estimates with those based on T_b signatures.

d. Algorithm sensitivities

Differences between the NSIDC and PMSTA melt onset estimates were examined in detail for an arbitrary year (1989) to assess effectiveness of the PMSTA's SAT threshold. Over one-third (38.8%) of the NSIDC melt onset estimates were dated earlier than the corresponding PMSTA estimates (regions ''D'' in Fig. 1 were excluded). The earlier NSIDC melt estimates tended to occur in the peripheral seas. For those pixels with earlier NSIDC melt dates, the corresponding daily IABP/POLES SAT data depicted thermal environments that were not conducive to onset of the melt season (Table 7). Application of the PMSTA's −5°C SAT threshold

TABLE 5. Mean annual differences in melt onset date, freeze onset date, and duration of the melt season between the PMSTA method and NSIDC (AHRA) method, and between the PMSTA method and the IABP/POLES SAT method, for the Northern Hemisphere, Arctic Ocean, and peripheral seas. Mean Δ = (PMSTA minus NSIDC) and (PMSTA minus IABP/POLES). SE is standard error of the mean. Significant ($S \geq$ 95%) mean differences (paired t test) are shown in bold type.

	PMSTA − NSIDC (1979–1998)		PMSTA−IAPB/POLES (1979–2000)					
	Melt onset		Melt onset		Freeze onset		Melt duration	
Region	Mean Δ	SE	Mean Δ	SE	Mean Δ	SE	Mean Δ	SE
Northern Hemisphere	**10.5**	1.26	**−5.9**	0.56	**10.8**	0.61	**16.8**	0.83
Barents–Kara Seas	**21.1**	3.51	**−17.8**	1.58	**13.7**	1.35	**31.5**	2.20
Chukchi Sea	**10.3**	2.57	**−7.6**	1.69	**8.6**	1.40	**15.7**	1.85
Laptev Sea	**10.0**	3.35	**−6.7**	1.00	**11.9**	1.72	**18.6**	1.85
East Siberian Sea	2.5	1.46	0.7	1.45	**10.1**	1.25	**9.4**	1.73
Arctic Ocean	**3.1**	0.92	1.1	0.75	**8.8**	0.85	**7.3**	1.08
Perennial ice	**0.9**	0.37	**5.3**	0.89	**4.7**	1.13	**−0.5**	1.32
Annual ice	**4.9**	1.35	−1.6	0.83	**11.8**	0.86	**11.7**	1.09

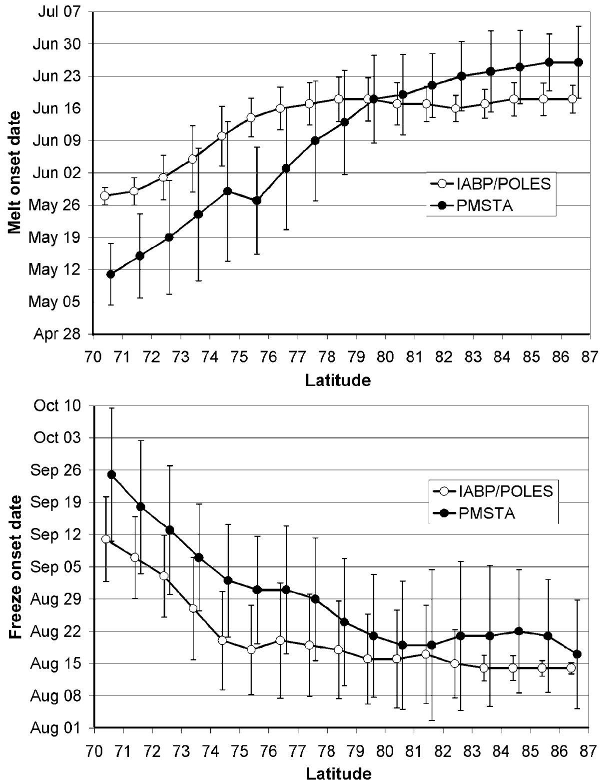

FIG. 8. Mean (top) melt onset date and (bottom) freeze onset date estimated by the PMSTA and IABP/POLES algorithms within 1° latitudinal zones, Arctic Ocean area, 1996.

clearly delayed the estimated melt dates compared to the NSIDC dataset, and arguably shifted the dates toward periods with more plausible thermal conditions.

The IABP/POLES SAT method was more sensitive than the PMSTA to the choice of algorithm thresholds (Table 8). Varying the IAPB/POLES SAT threshold by only ±0.5°C caused average melt and freeze estimates in 1989 to vary 4–12 days. Because the IABP/POLES SAT dataset was derived primarily by broad-scale interpolation of data from a sparse network of drifting stations (Rigor et al. 2000), small changes to the SAT thresholds caused relatively large spatial and temporal changes to the algorithm's output. In contrast, the PMSTA melt onset estimates were comparatively insensitive to all thresholds (T_b and SAT), indicating the −5°C SAT threshold provided sufficient margin for robust detection of the T_b melt signature. However, the PMSTA freeze estimates were influenced more by the SAT threshold, evidenced by a +1.0°C offset causing freeze to advance several days, while offsetting each T_b threshold had little effect (Table 8). Since microwave detection of freeze onset is more problematic because latent heat stored in brine pockets and melt ponds cause false T_b signatures during the freezing process (Rigor et al. 2000), the PMSTA had greater dependence on, and sensitivity to, the SAT threshold.

The SMMR–SSM/I microwave sensors are very sensitive to emissivity changes caused by the presence of small amounts of liquid water in the snowpack and on the sea ice surface (Comiso and Kwok 1996; Anderson 1997). Accordingly, brightness temperatures changed significantly during melt and freeze periods. These changes were approximately similar for snow on annual and perennial sea ice (Anderson 1977; Anderson and Drobot 2001), which provided signatures for detecting melt and freeze onset dates throughout the Arctic. Daily averaged brightness temperatures were used in this study because significant T_b variations between daytime melting and nighttime refreezing required a single daily response to consistently detect the melt and freeze signatures.

While SMMR–SSM/I passive microwave data provide scientists with comprehensive, broad-scale characterizations of the global sea ice cover, there are problems associated with developing consistent brightness temperature datasets for long-term studies. Precise adjustments are critical when standardizing brightness temperatures between the SMMR, and SSM/I, *F8*, *F11*, and *F13* satellite sensors. Recent studies have demonstrated that the magnitude of natural environmental changes can be within the tolerances of instrument calibrations, and that differences between sensors may be large enough to impact the monitoring of global sea ice

TABLE 6. Mean differences in melt onset and freeze onset dates estimated by different algorithms and data for selected case sites (N = 22) in the northern Beaufort Sea region dominated by perennial ice, 1992. Significant ($S \geq 95\%$) mean differences (paired t test) and linear latitudinal difference trends are shown in bold type. Drobot and Anderson (2001a) is denoted as D&A (2001a).

Parameter	Comparison	Mean Δ ± SE (days)	Latitudinal Δ trend [days (lat)$^{-1}$]
Melt onset	PMSTA − Smith (1998a)	**2.82 ± 0.70**	0.13 ± 0.28
	PMSTA − D&A (2001a)	0.95 ± 0.77	−0.31 ± 0.30
	PMSTA − IABP/POLES	1.09 ± 0.94	**0.91 ± 0.32**
	IABP/POLES − Smith (1998a)	**1.73 ± 0.54**	**−0.78 ± 0.13**
	IABP/POLES − D&A (2001a)	−0.14 ± 0.85	**−1.22 ± 0.21**
Freeze onset	PMSTA − Smith (1998a)	−0.50 ± 0.96	−0.19 ± 0.39
	PMSTA − IABP/POLES	1.50 ± 0.98	0.79 ± 0.36
	IABP/POLES − Smith (1998a)	**−2.00 ± 0.74**	**−0.98 ± 0.21**

TABLE 7. Mean melt onset date (Julian) and corresponding mean daily IABP/POLES SAT (°C) for pixels where the NSIDC melt date estimate preceded the PMSTA estimate, 1989.

Region	N (pixels)	Percent of total area	NSIDC melt onset		PMSTA melt onset	
			Date	SAT	Date	SAT
Barents–Kara Seas	1100	87.6	124	−8.8	141	−3.0
Chukchi Sea	436	77.7	107	−14.9	139	−4.7
Laptev Sea	441	51.6	151	−5.6	160	−2.0
East Siberian Sea	271	65.8	142	−9.0	153	−1.4
Arctic Ocean	2591	32.5	151	−6.4	156	−1.8
Perennial ice	346	10.6	159	−1.3	160	−0.5
Annual ice	2245	47.8	145	−7.2	154	−2.0

trends (Maslanik et al. 1996; Bjorgo et al. 1997; Stroeve et al. 1998). Recently published intersatellite calibration adjustments, analogous to those used by Drobot and Anderson (2001a), were used in this study for comparability with the NSIDC melt onset dataset (Drobot and Anderson 2001c).

We found that the PMSTA and AHRA (NSIDC) methods were sensitive to small offsets in the slope and intercept terms used for intersatellite T_b calibrations (Table 9). The calibration offsets we investigated (±0.02 slope, ±2K intercept) were chosen to depict modest uncertainty in the operational published values (Jezek et al. 1991; Stroeve et al. 1998; Abdalati et al. 1995). Sensitivity results for 1989 (Table 9), based on data from the calibration reference instrument (*F8* SSM/I), were generally similar to the results for other years and instruments. The notable sensitivity of melt and freeze estimates to small changes in the T_b calibration coefficients emphasizes the importance of accurate continuity across the multisensor datasets, as well as the risk of comparing results that were based on different calibration methods.

4. Conclusions

This investigation of sea ice melt dynamics over the last 23 years contributes to a growing body of scientific literature reporting linkages between Arctic sea ice and atmospheric processes. Significantly longer melt seasons in the eastern Siberian Arctic were coincident with prevalent low-pressure systems characteristic of high-index AO conditions. In the northern East Siberian and Chukchi Seas, mean annual melt duration was 2–3 weeks longer after the AO shifted to a more positive phase, compared to prior years. Other studies have found corroborating relationships in predominantly annual ice regions of the eastern Arctic, including warmer surface air temperatures, earlier melt onset, and reduced ice extent. Cyclonic atmospheric circulation and sea ice motion anomalies during high-index AO winters are thought to establish a suite of dynamic and thermodynamic processes that persist into the spring and promote earlier melt, enhanced heat flux, positive ice-albedo feedbacks, and delayed freeze. The observed northward expansions of earlier melt onset and later freeze in the Siberian sector of the Arctic Ocean during 1989–2001 were consistent with hypothesized processes of heat exchange as facilitated by atmospheric and sea ice circulation patterns during high-index AO conditions.

The Passive Microwave Surface Temperature Algorithm (PMSTA) arguably improves upon previously published methods for estimating sea ice melt and freeze dates. The PMSTA is applicable to both perennial and annual ice types, it employs SAT data to circumvent anomalous estimates arising from false T_b signatures, and it is relatively insensitive to the choice of algorithm thresholds. However, it is difficult to evaluate accuracies among different detection algorithms because robust

TABLE 8. Mean changes in the estimated melt and freeze onset dates (days) for perennial (MY) and annual (FY) sea ice (1989) after offsets were individually applied to the original PMSTA and IABP/POLES algorithm thresholds.

Method	Parameter	Melt onset Original value	Melt onset Offset	Melt onset Mean date MY	Melt onset Mean date FY	Freeze onset Original value	Freeze onset Offset	Freeze onset Mean date MY	Freeze onset Mean date FY
IABP/POLES	T_{onset}	−1.0°C	−0.5°C	−3.7	−4.3	−1.0°C	−0.5°C	5.0	4.2
			+0.5°C	12.1	8.3		+0.5°C	−7.9	−7.1
PMSTA	Δmin	−10.0K	−2.0K	0.0	0.4	−3.0K	−1.0K	0.0	0.0
			+2.0K	0.0	−0.2		+1.0K	0.0	0.0
	Δmax	4.0K	−1.0K	2.3	1.1	5.0°	−1.0K	−0.3	−0.2
			+1.0K	−1.4	−1.0		+1.0K	0.3	0.2
	R_{min}	7.5K	−1.0K	−0.8	−0.7	7.5K	−1.0K	0.1	0.1
			+1.0K	0.8	0.7		+1.0K	0.0	0.0
	T-SAT	−5.0°C	−1.0°C	0.0	−0.7	−2.0°C	−1.0°C	0.5	1.1
			+1.0°C	0.3	1.2		+1.0°C	−3.8	−3.2

TABLE 9. Mean changes (days) in melt and freeze onset dates, for perennial and annual sea ice (1989), when SSM/I intersatellite *Tb* calibration coefficients (slope and intercept, channel in GH_z and polarization as shown) were individually varied before input to the PMSTA and our realization of the Advanced Horizontal Range Algorithm (AHRA*).

		Melt onset date				Freeze onset date	
		Perennial		Annual		Perennial	Annual
Coefficient	Value	PMSTA	AHRA*	PMSTA	AHRA*	PMSTA	PMSTA
37 H intercept	−2K	5.3	3.8	3.2	5.2	−0.7	−0.5
	+2K	−2.6	−2.9	−1.8	−3.0	0.7	0.5
19 H intercept	−2K	−2.6	−2.9	−1.8	−3.0	0.7	0.5
	+2K	5.3	3.8	3.2	5.2	−0.7	−0.5
37 H slope	0.98	13.9	13.1	10.8	15.8	−1.6	−1.0
	1.02	−5.3	−6.3	−3.4	−9.0	1.3	1.0
19 H slope	0.98	−5.3	−6.1	−3.4	−8.4	1.3	1.0
	1.02	13.9	13.1	10.6	15.5	−1.6	−1.0

validation data are lacking, and different algorithms target different geophysical thresholds during the melt and freeze transitions. More research is needed to develop new invariant methods to slight adjustments of the T_b calibration coefficients and algorithm thresholds.

This study capitalized on the historic value of the SMMR–SSM/I data archive to facilitate comparison and integration with other long-term ocean–land–atmosphere investigations. Sensitivity analyses indicated that modest changes to the coefficients used for SMMR–SSM/I intersensor calibration caused estimated melt and freeze dates to vary ± 1 week, which rivaled sensitivity of the algorithm thresholds, and reconfirmed the importance of accurately standardizing T_b measurements among different satellite instruments.

Length of the summer sea ice melt season is an important and responsive indicator of Arctic warming. Satellite monitoring of sea ice parameters and melt processes is critical for better understanding temperature–albedo feedback mechanisms, climate changes, and for improving climate models. More research is needed to understand how interactions among atmospheric circulation, sea ice motion, and sea ice melt dynamics in the Arctic could significantly affect the behavior of ice–albedo feedbacks and ocean–atmosphere heat fluxes in global climate models.

Acknowledgments. This work was carried out with the support of the International Arctic Research Center, University of Alaska Fairbanks, the NATO Scientific and Environment Affairs Division (Collaborative Linkage Grant EST.CLG.978230), and the USGS Alaska Science Center. We would like to acknowledge the National Snow and Ice Data Center (University of Colorado) for providing the SMRR and SSM/I Daily Polar Gridded T_b and Sea Ice Concentrations, and the Polar Science Center, Applied Physics Laboratory (University of Washington) for providing IABP/POLES SAT data. We thank J. Walsh and an anonymous peer reviewer for their very constructive comments and recommendations.

REFERENCES

Abdalati, W., and K. Steffen, 1997: Snowmelt on the Greenland ice sheet as derived from passive microwave satellite data. *J. Climate,* **10,** 165–175.

——, ——, C. Otto, and K. C. Jezek, 1995: Comparison of brightness temperatures from SSM/I instruments on the DMSP F8 and F11 satellites for Antarctica and the Greenland ice sheet. *Int. J. Remote Sens.,* **16,** 1223–1229.

Anderson, M. R., 1997: Determination of a melt-onset data for Arctic sea-ice regions using passive microwave data. *Ann. Glaciol.,* **25,** 382–387.

——, and S. D. Drobot, 2001: Spatial and temporal variability in snowmelt onset over Arctic sea-ice. *Ann. Glaciol.,* **33,** 74–78.

Barber, D. G., S. P. Reddan, and E. F. LeDrew, 1995: Statistical characterization of the geophysical and electrical properties of snow on landfast first-year sea ice. *J. Geophys. Res.,* **100** (C2), 2673–2686.

Barry, R. G., 1996: The parametrization of surface albedo for sea ice and its snow cover. *Prog. Phys. Geogr.,* **20,** 61–77.

——, M. C. Serreze, J. A. Maslanik, and R. H. Preller, 1993: The Arctic sea ice–climate system: Observations and modeling. *Rev. Geophys.,* **31,** 397–422.

Belchansky, G. I., and D. C. Douglas, 2002: Seasonal comparisons of sea ice concentration estimates derived from SSM/I, OKEAN, and RADARSAT data. *Remote Sens. Environ.,* **81,** 67–81.

Bjorgo, E., O. M. Johannessen, and M. W. Miles, 1997: Analysis of merged SMMR–SSM/I time series of Arctic and Antarctic sea-ice parameters 1978–1995. *Geophys. Res. Lett.,* **24,** 413–416.

Cavalieri, D. J., C. L. Parkinson, P. Gloersen, J. C. Comiso, and H. J. Zwally, 1999: Deriving long-term time series of sea ice cover from satellite passive-microwave multisensor data sets. *J. Geophys. Res.,* **104** (C7), 15 803–15 814.

Chapman, W. L., and J. E. Walsh, 1993: Recent variations of sea ice and air temperature in high latitudes. *Bull. Amer. Meteor. Soc.,* **74,** 33–47.

Comiso, J. C., 1990–2001: DMSP SSM/I daily polar gridded sea ice concentrations. National Snow and Ice Data Center, Boulder, CO, CD-ROM.

——, 2001: Satellite-observed variability and trend in sea-ice extent, surface temperature, albedo and clouds in the Arctic. *Ann. Glaciol.,* **33,** 457–473.

——, and R. Kwok, 1996: Surface and radiative characteristics of the summer Arctic sea ice cover from multisensor satellite observations. *J. Geophys. Res.,* **101** (C12), 28 397–28 416.

Crane, R. G., and M. R. Anderson, 1994: Springtime emissivity changes in the southern Kara Sea. *J. Geophys. Res.,* **99** (C7), 14 303–14 309.

Curry, J. A., J. L. Schramn, and E. E. Ebert, 1995: On the ice albedo climate feedback mechanism. *J. Climate,* **8,** 240–247.

Deser, C., J. E. Walsh, and M. S. Timlin, 2000: Arctic sea ice variability in the context of recent atmospheric circulation trends. *J. Climate,* **13,** 617–633.

Drobot, S. D., and M. R. Anderson, 2001a: An improved method for determining snow melt-onset dates over Arctic sea-ice using scanning multichannel microwave radiometer and Special Sensor Microwave/Imager data. *J. Geophys. Res.,* **106** (D20), 24 033–24 049.

——, and ——, 2001b: Comparison of interannual snowmelt-onset dates with atmospheric conditions. *Ann. Glaciol.,* **33,** 79–84.

——, and ——, 2001c: Snow melt onset over Arctic sea ice from SMMR and SSM/I Tbs. National Snow and Ice Data Center, Boulder, CO, CD-ROM.

El Naggar, S., C. Garrity, and R. O. Ramsier, 1998: The modeling of sea ice melt-water ponds for the high Arctic using an airborne line scan camera, and applied to the Satellite Special Sensor Microwave/Imager (SSM/I). *Int. J. Remote Sens.,* **19,** 2372–2394.

Gloerson, P., D. Cavalieri, W. J. Campbell, and J. Zwally, 1990: *Nimbus-7* SMMR polar radiances and Arctic and Antarctic sea ice concentrations. National Snow and Ice Data Center, Boulder, CO, CD-ROM.

——, C. L. Parkinson, D. J. Cavalieri, J. C. Comiso, and H. J. Zwally, 1999: Spatial distribution of trends and seasonality in the hemispheric sea ice covers: 1978–1996. *J. Geophys. Res.,* **104** (C9), 20 827–20 835.

Ikeda, M., J. Wang, and J.-P. Zhao, 2001: Hypersensitive decadal oscillations in the Arctic/subarctic climate. *Geophys. Res. Lett.,* **28,** 1275–1278.

Jezek, K. C., C. Merry, D. Cavalieri, S. Grace, J. Bedner, D. Wilson, and D. Lampkin, 1991: Comparison between SMMR and SSM/I passive microwave data collected over Antarctic ice sheet. Ohio State University Byrd Polar Research Tech. Rep. 91–03, 62 pp.

Maslanik, J. A., and J. Stroeve, 1990–2001: DMSP SSM/I daily polar gridded brightness temperatures. National Snow and Ice Data Center, Boulder, CO, CD-ROM.

——, M. C. Serreze, and R. G. Barry, 1996: Recent decreases in Arctic summer ice cover and linkages to atmospheric circulation anomalies. *Geophys. Res. Lett.,* **23,** 1677–1680.

Mysak, L. A., and S. A. Venegas, 1998: Decadal climate oscillations in the Arctic: A new feedback loop for atmosphere–ice–ocean interactions. *Geophys. Res. Lett.,* **25,** 3607–3610.

Onstott, R. G., T. C. Grenfell, C. Matzler, C. A. Luther, and E. A. Svendsen, 1987: Evolution of microwave sea ice signatures during early summer and midsummer in the marginal ice zone. *J. Geophys. Res.,* **92** (C7), 6825–6835.

Parkinson, C. L., 1992: Spatial patterns of increases and decreases in the length of the sea ice season in the north polar region. *J. Geophys. Res.,* **97** (C9), 14 377–14 388.

——, D. J. Cavalieri, P. Gloersen, H. J. Zwally, and J. C. Comiso, 1999: Arctic sea ice extends, areas, and trends, 1978–1996. *J. Geophys. Res.,* **104** (C9), 20 837–20 256.

Perovich, D. K., 1996: *The Optical Properties of Sea Ice. CRREL Monogr.,* No. 96-1, U.S. Army Cold Regions Research and Engineering Laboratory, 25 pp.

Pettersson, M. I., J. Askne, and D. J. Cavalieri, 1996: SAR observation of Arctic freeze-up compared to SSM/I during ARCTIC'91. *Int. J. Remote Sens.,* **17,** 2603–2624.

Rigor, I. G., R. L. Colony, and S. Martin, 2000: Variations in surface air temperature observations in the Arctic, 1979–97. *J. Climate,* **13,** 896–914.

——, J. M. Wallace, and R. L. Colony, 2002: Response of sea ice to the Arctic Oscillation. *J. Climate,* **15,** 2648–2663.

Serreze, M. C., J. A. Maslanik, G. R. Scarfen, and R. G. Barry, 1993: Interannual variations in snow melt over Arctic sea ice and relationships to atmospheric forcing. *Ann. Glaciol.,* **17,** 327–331.

——, ——, J. R. Key, R. F. Kokaly, and D. A. Robinson, 1995: Diagnosis of the record minimum in Arctic sea ice area during 1990 and associated snow cover extremes. *Geophys. Res. Lett.,* **22,** 2183–2186.

Smith, D. M., 1998a: Observation of perennial Arctic sea ice melt and freeze-up using passive microwave data. *J. Geophys. Res.,* **103** (C12), 27 753–27 769.

——, 1998b: Recent increase in the length of the melt season of perennial Arctic sea ice. *Geophys. Res. Lett.,* **25,** 655–658.

Steele, M., and Coauthors, 2001: Adrift in the Beaufort Gyre: A model intercomparison. *Geophys. Res. Lett.,* **28,** 2935–2938.

Stroeve, J., J. Maslanik, and L. Xiaoming, 1998: An intercomparison of DMSP F11- and F13-derived sea ice products. *Remote Sens. Environ.,* **64,** 132–152.

Thompson, D. W. J., and J. M. Wallace, 1998: The Arctic Oscillation signature in the wintertime geopotential height and temperature fields. *Geophys. Res. Lett.,* **25,** 1297–1300.

——, and ——, 2000: Annular modes in the extratropical circulation. Part I: Month-to-month variability. *J. Climate,* **13,** 1000–1016.

Walsh, J. E., W. L. Chapman, and T. L. Shy, 1996: Recent decrease of sea level pressure in the central Arctic. *J. Climate,* **9,** 480–485.

Winebrenner, D. P., E. D. Nelson, R. Colony, and R. D. West, 1994: Observation of melt onset on multiyear Arctic sea ice using the *ERS-1* synthetic aperture radar. *J. Geophys. Res.,* **99** (C11), 22 425–22 441.

Yackel, J. J., and G. G. Barber, 2000: Melt ponds on sea ice in the Canadian Archipelago: 1. On the use of RADARSAT-1 synthetic aperture radar for geophysical inversion. *J. Geophys. Res.,* **105** (C9), 22 061–22 070.

Yi, D., L. A. Mysak, and S. Venegas, 1999: Decadal-to-interdecadal fluctuations of Arctic sea-ice cover and the atmospheric circulation during 1954–1994. *Atmos.–Ocean,* **37,** 389–415.

Zhang, J., D. Rothrock, and M. Steele, 2000: Recent changes in the Arctic sea ice: The interplay between ice dynamics and thermodynamics. *J. Climate,* **13,** 3099–3114.